

Article

Design of Continuous Kneading System for Active Anode Material Fabrication Using Retrofitted Assembly of Co-Rotating Screw Extruder

Gang-Ho Lee ¹, Hyenoseok Yi ² , Hye-Ryeong Cho ³, Yu-Jin Kim ³, Sei-Min Park ¹, Seong-Jin Yoon ³, Dong-Jin Seo ³, Kyeongseok Oh ⁴ , Jeong-Mi Yeon ⁵, Sun-Yong Choi ⁵, Seong-Ho Yoon ^{2,*}  and Joo-Il Park ^{3,*}

¹ Carbon Materials Research Group, Research Institute of Industrial Science & Technology (RIST), Pohang 37673, Republic of Korea

² Institute for Materials Chemistry and Engineering, Kasuga 816-8580, Fukuoka, Japan; yi@cm.kyushu-u.ac.jp

³ Department of Chemical & Biological Engineering, Hanbat National University, Daejeon 34158, Republic of Korea; tjdwls7856@gmail.com (S.-J.Y.)

⁴ Department of Chemical and Biological Engineering, Inha Technical College, Incheon 22212, Republic of Korea

⁵ Division of Plasma Convergence R&D, Cheorwon Plasma Research Institute, Cheorwon 24047, Republic of Korea; jmyeon@cpri.re.kr (J.-M.Y.); sychoi@cpri.re.kr (S.-Y.C.)

* Correspondence: yoon@cm.kyushu-u.ac.jp (S.-H.Y.); jipark94@hanbat.ac.kr (J.-I.P.); Tel.: +81-92-583-7959 (S.-H.Y.); +82-42-821-1530 (J.-I.P.)

Abstract: As the demand for artificial graphite for lithium-ion battery (LIB) anode materials is on the rise, technologies for optimizing the manufacturing processes and reducing the production costs of artificial graphite are crucial. At the same time, globally, regulations on the generation of harmful volatile substances during the artificial graphite production process are also becoming increasingly stringent. In this study, we focused on a continuous kneading process that minimizes the emission of volatile substances during the manufacturing of artificial graphite. To this end, a carbonized material was first prepared from a mixture of needle coke and binder pitch and processed at 3200 °C using two types of co-rotating twin-screw extruder-based continuous kneading equipment to ultimately obtain artificial graphite. The physical properties of the carbonized as well as graphitized materials were analyzed, which revealed the superior performance of the LIB anode material, namely a discharge capacity of greater than or equal to 350 mAh/g, and an initial efficiency of 91% or higher. Thus, a continuous kneading manufacturing process that emits less harmful volatile substances and provides artificial graphite with sufficient battery performance was demonstrated.

Keywords: artificial graphite; kneading process; twin-screw extruder; anode material; lithium ion battery



Citation: Lee, G.-H.; Yi, H.; Cho, H.-R.; Kim, Y.-J.; Park, S.-M.; Yoon, S.-J.; Seo, D.-J.; Oh, K.; Yeon, J.-M.; Choi, S.-Y.; et al. Design of Continuous Kneading System for Active Anode Material Fabrication Using Retrofitted Assembly of Co-Rotating Screw Extruder. *Processes* **2023**, *11*, 2660. <https://doi.org/10.3390/pr11092660>

Academic Editor: Mingxia Gao

Received: 20 June 2023

Revised: 30 July 2023

Accepted: 21 August 2023

Published: 5 September 2023



Copyright: © 2023 by the authors. Licensee MDPI, Basel, Switzerland. This article is an open access article distributed under the terms and conditions of the Creative Commons Attribution (CC BY) license (<https://creativecommons.org/licenses/by/4.0/>).

1. Introduction

Lithium-ion batteries (LIBs) are used in a wide range of devices from simple smartphones to more sophisticated electric vehicles. The use of LIBs is expected to rapidly increase commensurate with consumer demands. The key features of LIB include high energy density and initial Coulombic efficiency (ICE) [1–12]. The first technological breakthrough in LIBs was achieved as early as the 1970s after the discovery of LiC₆ compounds supported by graphite layers in a charged state [13–15]. In general, anode precursors are derived from carbon materials, such as soft and hard carbons, artificial and natural graphite, and relevant derivatives. Artificial graphite from coal tar or petroleum-derived precursors [16] has played an essential role in the LIB market since its invention in the 1990s [17–19]. Due to its intrinsic and unique molecular structure, artificial graphite can provide highly volatile Li ions in multiple stacks of graphene sheets [20–22]. Recent research on typical artificial graphite revealed a discharge capacity of more than 320 mAh/g [23].

However, there are numerous challenges to the mass production of artificial graphite: first, buyers still expect to purchase it at low prices; second, with electric vehicles flooding the automotive market, battery cell makers have to cope with the down-pricing of the cells. Two recognizable market players, Shanshan Tech Co., Ltd., and Jiangxi Zichen Technology Co., Ltd. have been using their own powder processing technologies that lower the production cost while maintaining a low surface area of the active anode materials.

Currently, twin-screw extruders are widely used in various industries, such as food processing [24–28], ceramics [29–32], and polymers [33–36]. However, research on twin-screw extruders optimized for manufacturing artificial graphite is scarce; to date, artificial graphite has been simply pulverized and sold as extruded graphite. Therefore, developing an optimal extruder for the artificial graphite manufacturing process offers significant potential for LIB manufacturing. Another manufacturing process relevant to artificial graphite manufacturing, namely the kneading process, is considered an expensive operation. For instance, a typical kneading process, currently in practice, requires more than 12 h, including the core process, cooling, and cleansing steps. Furthermore, from the perspective of environmental safety, it is considered a highly polluting activity by relevant government agencies, as the current technologies inevitably emit significant amounts of unhealthy fumes during the charging and discharging of feeds.

An exemplary design of the kneading assembly, which has achieved effective results for manufacturing graphite for battery anodes, employs continuously operated co-rotating twin-screw extruders [37]. Herein, two distinct and parallel co-rotating twin-screw extruders, the KRC-S2 model (Kurimoto, Ltd., Japan) and CHT-20 model (Nanjing Cowin Extrusion Machinery Co., Ltd., China), were selected and evaluated. The KRC-S2 model had an axis dimensional ratio of 44:5 (440 and 50 mm in length and diameter, respectively), rotating at 30 rpm (Figure 1a). The system was equipped with a reverse helical-shaped screw paddle at its end so that additional compactness could be applied to the feed before being discharged. The sample discharging outlet was placed on the bottom side of the barrel, where the sliding gate adjusted the opening time. In contrast, the CHT-20 model was built with an axis dimensional ratio of 44:1 (968 and 22 mm in length and diameter, respectively) (Figure 1b). Thus, the CHT-20 model was twice as long as the KRC-S2 model. In addition, the CHT-20 model was set to 300 rpm, which was advantageous for avoiding feed clogging. To compare the two models, their kneading performances were evaluated at the same residence time of 20 min at 250 °C. CHT-20 demonstrated superior performance in the secondary particle expansion of D50. Subsequently, a retrofit design was created by installing an additional component in CHT-20 (Figure 2). Here, two twin-screw extruders were connected by a single screw feeder so that the outlet of the first extruder and the inlet of the second extruder overlapped to prevent fume discharge. While the same axis diameter of 22 mm was maintained, the length-to-diameter ratio increased from 44:1 to 64:1 (that is, 1408 and 22 mm in length and diameter, respectively). The conveying, mixing, and engaging elements were made of $W_6Mo_5Cr_4V_2$, with 40CrNiMo selected as the core material. Each barrel comprised eight sections with a heating capability that could raise the temperatures to 400 °C. With each heating unit length being 160 mm, a total heating length of 1280 mm was available. Considering the smooth running of a powdered mix of coke and pitch under high pressure, a single screw vertical feeder (power: 0.18 kW and output speed: up to 50 rpm) was placed in such a way that the premix could go directly to the rotating axis by force. This was to avoid clogging under lower rpms, for example, 20 rpm (1/15th compared to the original setting of 300 rpm).

The objective of this study was to design a continuous kneading process that minimizes the release of harmful volatile materials. As mentioned earlier, various volatile materials and dust are generated during the artificial graphite manufacturing process. In an actual industrial setting, purifiers and dust collectors are utilized to mitigate pollution. As the need for eco-friendly technologies has grown worldwide, the demand for the minimization of volatile materials and dust generation in the manufacture of artificial graphite has also increased. Therefore, in this study, we developed an environmentally friendly optimal

continuous process based on twin-screw extruders for the artificial graphite manufacturing process. We also evaluated the electrochemical performance of an LIB anode manufactured from the artificial graphite thus obtained.

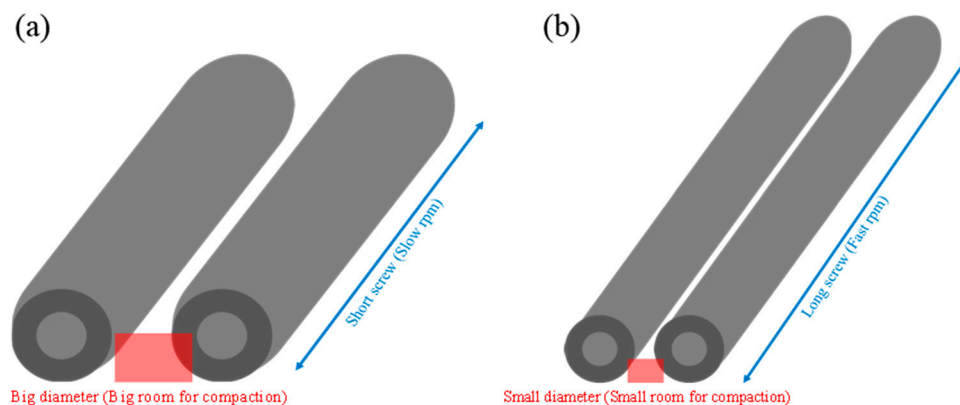


Figure 1. (a) KRC-S2 (In the courtesy of Kurimoto., Ltd.) and (b) HCT-20 (In the courtesy of Nanjing Cowin, Co., Ltd., China) kneader screw paddle composition.

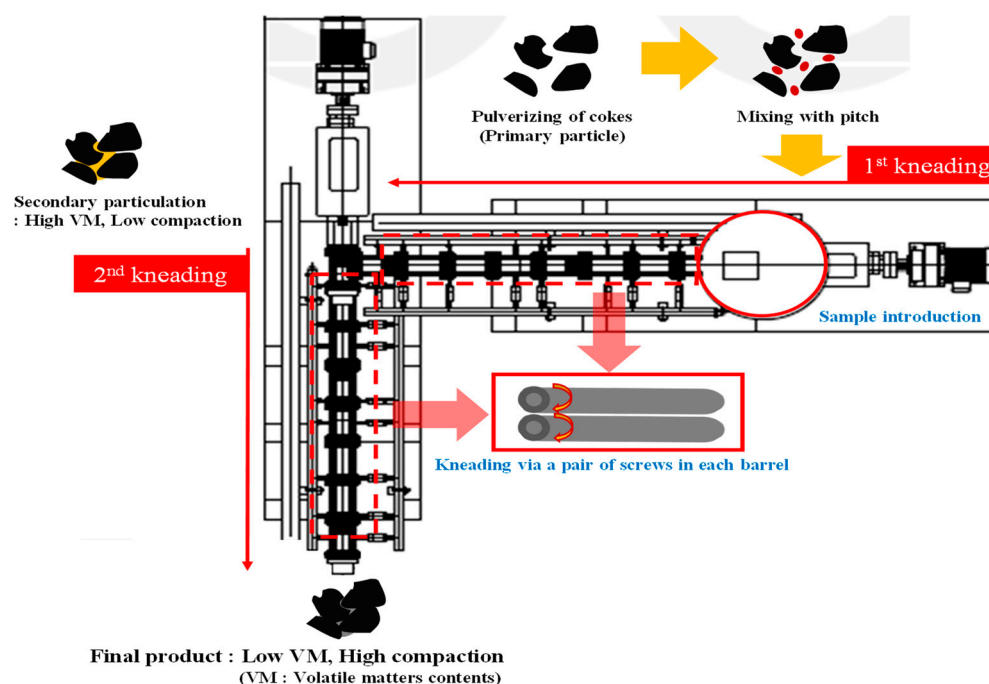


Figure 2. Retrofitted design of double twin-extruder type continuous kneader (In the courtesy of Nanjing Cowin, Co., Ltd., China).

2. Materials and Methods

2.1. Sample Preparation

2.1.1. Needle Cokes and Binding Pitch Composition

Two types of coal-derived needle cokes—green and calcined, prepared by POSCO MC Materials, Co., Ltd. (Republic of Korea). The cokes were pulverized to a particle size distribution of D50 set to approximately 10 μm . A petroleum-derived binding pitch (ZL250, RÜTGERS GmbH in Germany) with a softening temperature of 250 $^{\circ}\text{C}$ was premixed at room temperature with the needle cokes for 30 min at 30 rpm using a blade-type mixer (KRC-S2 sigma). The weight ratio of the cokes to the binding pitch was set to 1:0.12. The basic characteristic was summarized in Table 1.

Table 1. Characteristic of pitch binder, ZL250.

Pitch Binder	Source	QI (%)	Fixed Carbon (%)	Ash (%)	Sulfur (%)
ZL250	Petroleum	0.5	68	0.02	0.01

2.1.2. Comparison of Continuous Kneading Performance of KRC-S2 and CHT-20 Extruders

The premixed samples of cokes and pitch were fed to the aforementioned co-parallel rotating extruders once the barrel temperature reached 250 °C. A residence time of 20 min was stipulated. Considering the differences in the internal structural mechanisms of the two machines, the rotating speeds were controlled to 30 and 300 rpm for KRC-S2 and CHT-20, respectively, to maintain the same residence time; this also prevented the machines from clogging. The feeds were retrieved upon discharge and heat-treated at 3200 °C for 2 h. The particle size distributions of the feeds were measured at regular intervals.

2.1.3. Continuous Kneading by Retrofitted Double Co-Rotating Parallel Extruding System

The carbon/graphite precursor (1 kg) was mixed with a pitch binder (10–13.5% by extrapolation) at room temperature (25 °C) for 30 min. In other words, a pitch-binding material (10% by weight) was applied to the primary coke, whereas graphitized primary cokes were mixed with both 10% and 13.5% of the pitch binder for comparing the hydrophobic behavior of their surfaces after graphitization at 3200 °C. Particularly, a 2-L KRC-S2 sigma-blade-type kneader was used so that its twin rotors with opposite directions of rotation could enhance the uniform distribution of the feed. After being mixed at room temperature, the mixture was introduced into a retrofitted CHT-20 double barrel extruding type continuous kneader. The rotational speed of each screw was set to 20 rpm with a connecting single-screw feeder at 7 Hz so that the residence time was maintained at 20 min. The temperature was set to reach 90–100 °C above the softening point temperature of the binding pitch mixed feed; this would translate to 350 °C for a pitch with a softening point of 250 °C and 200 °C for a pitch with a softening point of 110 °C.

2.2. Characterization of Samples

2.2.1. Surface Properties

A surface character analyzer (3Flex, USA) was used to characterize the surface area and pore size distribution of the feed.

2.2.2. Particle Size Analysis

A particle size analyzer (Cilas 1090, CILAS, France) was used to measure the particle size distributions and spans.

2.2.3. Tap Density Measurement

The tap density was measured based on 20 g of each sample in the up- and down-tapping directions for 3000 counts.

2.2.4. Elemental Analysis

CHN elemental analysis (MT-5, Japan) was performed based on 1 g of each sample by heating the sample to 750 °C, at a heating rate of 5 °C/min.

2.2.5. X-ray Diffraction Measurement

The graphitization degree of the sample with the lowest surface area was selected for X-ray diffraction measurement (RIGAKU RINT Ultima+, Japan) at a narrow scan rate of 0.5 °/min (Cu-K α) in the range of 24–30° based on the Gakushin method and using Si as a reference.

2.2.6. Topological Characterization

A scanning electron microscope (SEM; JEM-ARM200F, JEOL, Japan) and a cold field emission gun (FEG) equipped with double Cs correctors were used for the topological characterization of the anode fabricated from artificial graphite.

2.3. Electrochemical Performance of the Artificial Graphite Anode

2.3.1. Cell Preparation

The anode was produced by uniformly mixing the anode active material, a binder (carboxy methyl cellulose and styrene butadiene rubber), and a conductive material (Super P) using distilled water so that its weight ratio became 97:2:1 (anode active material: binder: conductive material). The mixture was applied to a Cu current collector, compressed by a roll press, and dried under vacuum for 12 h at 100 °C. In this case, the electrode density was set to 1.5–1.6 g/cc. Using the respective constituent elements, a CR2032 half-coin cell was produced with Li as a counter electrode according to a conventional production method. A 1 mol. solution of LiPF₆ in a mixture of ethylene carbonate (EC) and dimethyl carbonate (DMC) at a 1:1 ratio by volume was used as the electrolyte.

2.3.2. Electrochemical Testing

The coin cell test was conducted under the following conditions: 0.1 C, 5 mV, and 0.005 C cut-off for charging; 0.1 C, and 1.5 V cut-off for discharging. The initial discharging capacity and ICE were measured.

3. Results and Discussion

3.1. Comparison of Continuous Kneading Performance of KRC-S2 and CHT-20 Extruders

The coal-derived needle cokes (both green and calcined) and petroleum-derived binder pitch were fed into the two aforementioned models of co-parallel rotating-type extruders, KRC-S2 and CHT-20, and the compounding effects were evaluated. The green needle cokes showed clear signs of secondary particle size expansion by both extruders. Here, the secondary particle size was categorized and evaluated as 10, 50, and 90 μm, which were named D10, D50, and D90, respectively. The expansion rates were increased for the three particle sizes (Figure 3a). Particularly, CHT-20 performed significantly better for D50 and D90. The D10 and D50 calcined needle cokes showed an inferior expansion in CHT-20 (Figure 3b); however, D90 size particles showed a higher expansion. Given the low wettability of the calcined cokes in the larger particle range, CHT-20 was more effective probably due to the longer barrel with a higher rotation speed of the paddle movement and smaller paddle depth, which led to fewer residues inside the barrel. Therefore, a relatively small-diameter rotating axis with a longer dimension operating at a faster rpm would be more effective in kneading as well as compounding the primary particles. Furthermore, it also generated larger and more desirable secondary particles. A larger axis can be predicted to translate into more redundant leftover particles that could result in additional unnecessary reactions with newly fed particles introduced later.

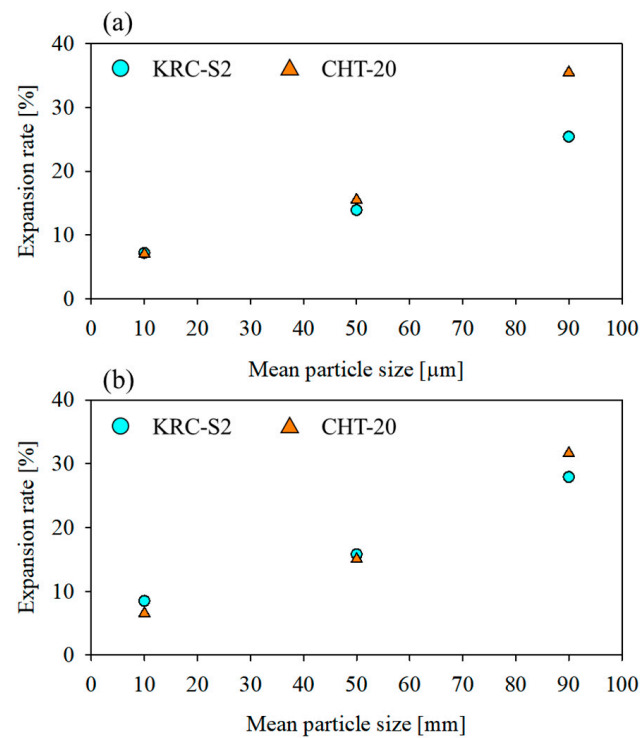


Figure 3. Secondary particle size expansion results of needle cokes with KRC-S2 and CHT-20 extruders: (a) green and (b) calcined.

3.2. Continuous Kneading Performance of the Retrofitted Consecutive Dual Co-Rotating Parallel Extruding System

After continuous kneading and compounding of the samples, an elemental analysis was conducted on the retrofitted machine. The results (Table 2) showed that the mixtures with a pitch having a higher softening point (250 °C) contained higher volatile matter. Notably, volatile matter was observed in the green coke-based mixture, regardless of whether isotropic or needle cokes were used. The calcined cokes also showed a similar tendency, albeit on a smaller scale. Thus, as expected, the volatile material content of the cokes was inevitable whether isotropic or needle cokes were used (Figure 4). The petroleum-derived pitch showed a uniform tendency of higher residual rate when combined with either of the coke materials, even though the pitch was treated at a temperature of 90–100 °C higher than the softening point. As mentioned earlier, the objective should be to eliminate the volatile matter generated from either the coke or pitch. This newly retrofitted system offers a solution to this issue. More pitch-derived binding materials could be used if higher speeds and limited internal dimensions of the barrel structure were incorporated into the retrofitted system. For example, a 10-μm petroleum-based pitch-binding sample with the highest tap density and lowest surface area presented the best electrode manufacturability because the active material could be coated well onto the Cu collector. A 6-μm petroleum-based pitch-binding sample, starting with a relatively smaller primary particle size of D50 of 6 μm, showed a less compounding effect, which translated to a lower tap density and surface area than the 10-μm petroleum-based pitch-binding sample. A 10-μm coal tar-based pitch-binding sample exhibited less compounding effect, probably owing to its less volatile content; however, it showed a relatively lower span. Moreover, it did not lead to a better tap density and surface area. It may be conjectured that some primary particles were intact and not kneaded, which might explain the slightly smaller D50. The 6-μm coal tar-based pitch-binding sample had the lowest tap density with a relatively high surface area while maintaining a fair amount of secondary particle size. Therefore, it may be concluded that only a limited number of primary particles passed through the kneading process to form proper secondary particles.

Table 2. Physical properties of calcined needle coke-based samples.

Primary Particle Size (D50, μm)	Pitch	Secondary Particle Size (D50, μm)	After Graphitization			
			Span	Tap Density (g/cc)	$d_{(002)}$ (nm)	Surface Area (m^2/g)
10	Pet.	15.24	1.40	0.82	0.3358	1.48
6	Pet.	8.90	1.48	0.63	0.3358	2.94
10	Coal	14.76	1.25	0.72	0.3358	1.96
6	Coal	10.91	1.34	0.62	0.3360	2.70

In relation to the volatile matter, the particle-size distribution measurement based on D50 volumetric analysis suggested that the parallel direction could help minimize volatile emissions, whereas the sample with a smaller amount of volatile matter had a larger particle size distribution. Therefore, a reduced amount of volatile matter was assumed to have been transformed, which formed a stronger bond with the other particles. Thus, comparatively larger secondary particles were generated. The coal-derived pitch samples evidently presented a higher rate of compounding effect, which could be mainly attributed to their innate higher beta-resin content compared to their petroleum-derived counterparts. Regardless of calcination, this tendency was maintained by both the needle and isotropic cokes. In terms of wettability, it could be concluded that the coal-derived coke agreed with the flows created by melting the same origin and coal-derived pitch-binding material.

To understand the relationship between the volatile matter and secondary particle expansion, a detailed analysis of the physical properties of the samples was conducted, considering various primary particle sizes and pitch-binding material types. Calcined cokes were selected to exclude the possible surface chemistry with pitch-binding materials derived from a coke structure.

In Figure 5, coal tar-based pitch-binding samples show apparently narrower spans, that is, $((D_{90}-D_{10})/D_{50})$ of less than 1.35; conversely, petroleum-based pitch-binding material samples showed higher values of tap density than their coal–tar-based counterparts. The primary particle size of the supporting cokes could be related to better electrode manufacturability. Such a phenomenon could be attributed to the severe centralization of the D50 particle size of the petroleum-based pitch groups. At the same time, coal tar-based pitch groups were expected to have a comparatively uniform distribution in all particle size distributions. All the samples were confirmed to possess reasonable graphitization degree values of less than or equal to 0.3360 nm, as measured by X-ray diffraction. The surface area suggested that it was strongly and inversely affected by the secondary particle size.

As confirmed by the images from SEM, all the samples showed evidence of agglomeration to form secondary particles. The petroleum-based pitch samples tended to possess less agglomerated morphologies in both 10 and 6 μm samples compared to their coal tar-based counterparts (Figure 6). This was probably due to their lower fixed carbon ratio, which was associated with lower beta–resin content, that is, TI (toluene insoluble) minus QI (quinoline insoluble). The petroleum pitch samples had, in other words, less binding content, thereby having fewer leftover carbons after calcination. What remained after the calcination was crucial in bonding cokes together. The SEM images show fewer particles attached to one another compared to their coal–tar pitch counterparts. In detail, the following could be concluded:

(a) The particle agglomeration was uniform, with a small portion of non-agglomerated particles, which were believed to be effective in the smooth transfer of lithium ions during charging and discharging cycles; this was due to its well-kneaded structure with finer particles attached to and agglomerated on larger particles.

(b) The agglomeration of the particles showed a strong intensity in that the starting particle size D50 was 6 μm , and yet, its final aggregated shape showed a relatively higher degree of size expansion, which affirmed that such a high degree of bonding would provide more scope for charging and discharging; this could translate to a larger capacity. In other

words, smaller particles were attached to one another in such a way that the agglomerated particles could possess a proper passage and room for the charge and discharge of Li ions.

(c) The non-agglomerated particles were observed with a low degree of bonding (small number of agglomerated particles), which implied that the kneading effect was hardly seen in these particles. The majority of the particles were believed to be primary particles (non-agglomerated). The non-kneaded particles were scattered, which was not a good sign of kneading.

(d) Given that the sample started with a D50 of 6 μm , a certain degree of agglomeration could still be seen (partial kneading effect); therefore, it may be inferred that a number of particles were not agglomerated, thereby showing a wide particle-size distribution.

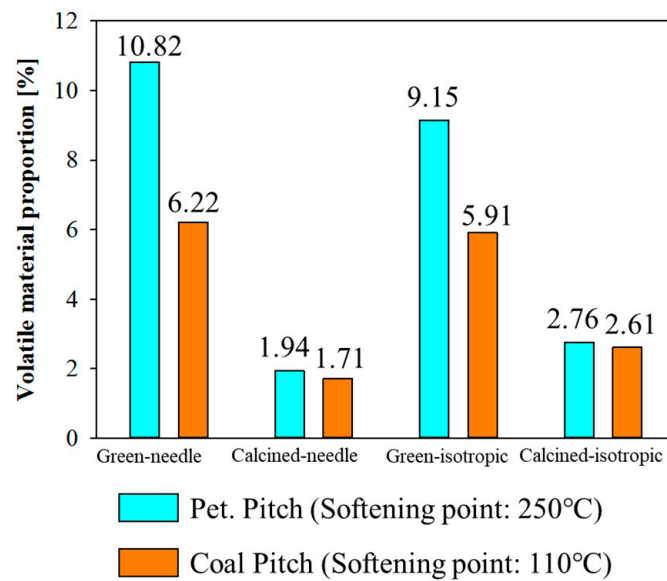


Figure 4. Comparison of volatile material proportion of coke after the continuous kneading of different combinations of needle cokes and pitch binders.

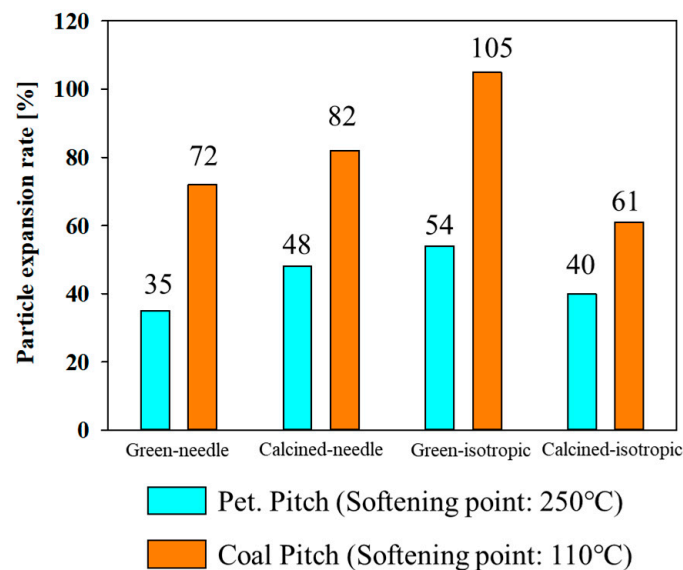


Figure 5. Comparison of particle size expansion rate after continuous kneading of different combinations of needle cokes and pitch binders.

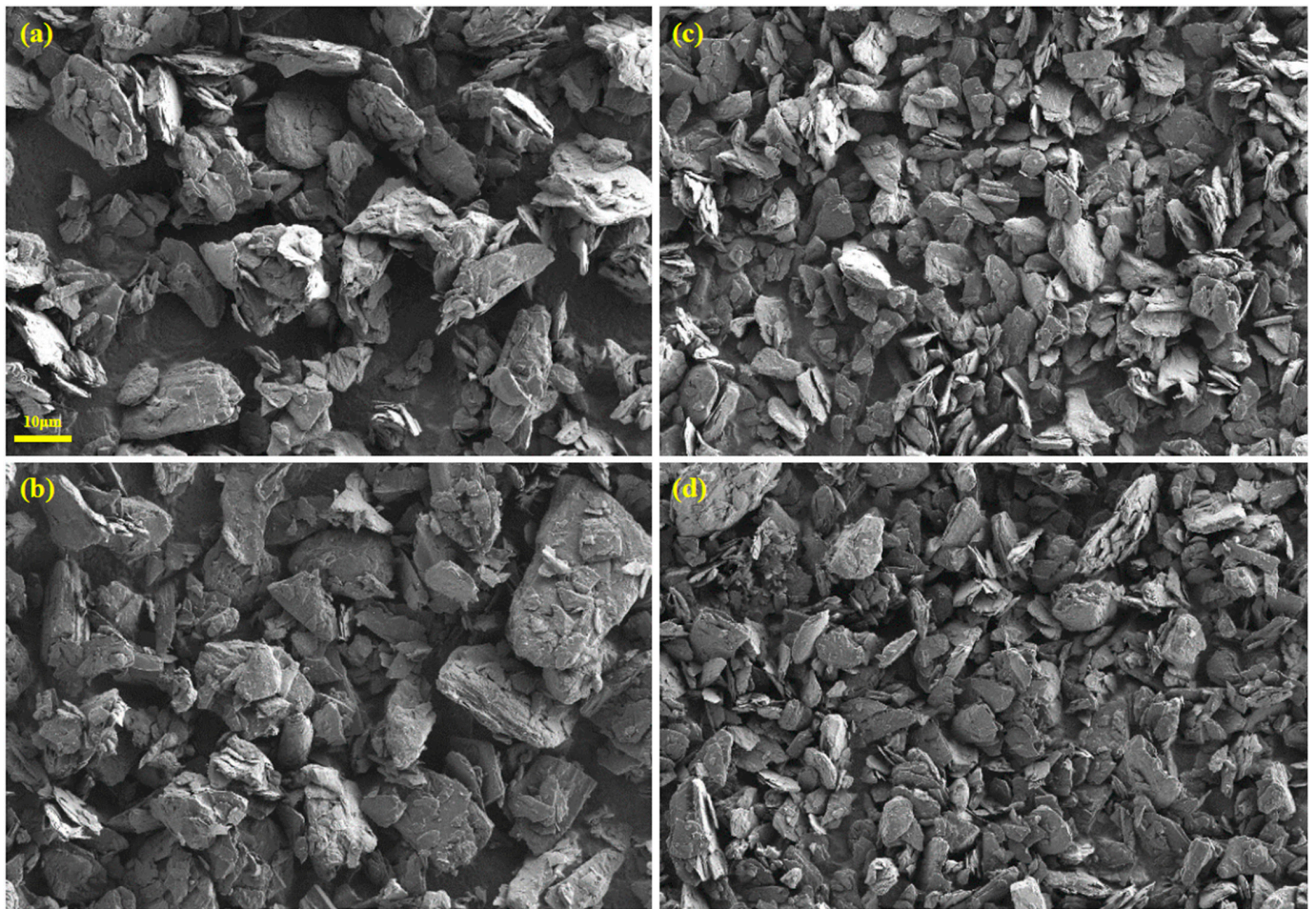


Figure 6. SEM photographs from graphitized active anode samples: (a) calcined needle coke with D50 particle size of 10 μm and petroleum-based pitch-binding material, (b) calcined needle coke with D50 particle size of 6 μm and petroleum-based pitch-binding material, (c) calcined needle coke with D50 particle size of 10 μm and coal-tar-based pitch-binding material, and (d) calcined needle coke with D50 particle size of 6 μm and coal-tar based pitch-binding material.

3.3. Electrochemical Testing Result

For calcined needle coke with D50 particle size, the LIB anode material test was performed. The third discharging capacity of all the D50 calcined needle cokes was more than 350 mAh/g (Figure 7, Table 3). This is acceptable based on the industrial standards of major LIB manufacturers. Only the calcined needle coke with a D50 particle size of 6 μm and a coal-tar-based pitch binder sample yielded an ICE of more than 90%. Evidently, the petroleum pitch-binding material created a positive bonding with the coal-derived calcined needle coke, which led to both a higher discharging capacity and ICE. This discharge capacity and ICE were significantly higher than 327 mAh/g and 81.6% of those of typical coal-derived artificial graphite [23]. The charging and discharging performances of all the aforementioned samples demonstrated a similar pattern of stable staging, with a plateau above the 20th cycle during charging. Similarly, uniformity in the discharging characteristics was observed.

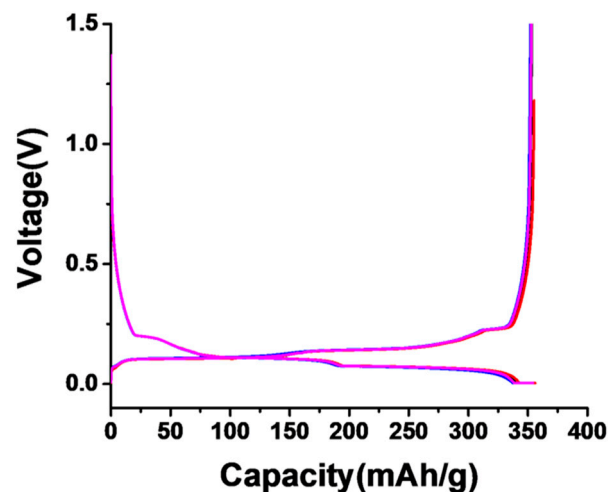


Figure 7. Charging and discharging cyclic characteristics: ■—calcined needle coke with D50 particle size of 10 μm and petroleum-based pitch-binding material, ■—calcined needle coke with D50 particle size of 6 μm and petroleum-based pitch-binding material, ■—calcined needle coke with D50 particle size of 10 μm and coal-tar-based pitch-binding material, and ■—calcined needle coke with D50 particle size of 6 μm and coal-tar-based pitch-binding material.

Table 3. Electrochemical testing results of calcined needle coke-based samples.

Primary Particle Size (D50, μm)	Pitch	Electrochemical Performance	
		Discharging Capacity (3rd, mAh/g)	ICE (1st, %)
10	Pet.	353.1	93.7
6	Pet.	355.0	92.7
10	Coal	350.3	92.4
6	Coal	352.9	91.5

Calcined-needle coke-based samples have proven the validity of the proposed system by producing better than average electrochemical performance, that is, a higher discharging capacity and ICE, thereby satisfying industrial standards. Moreover, evidently, the proportions of the cokes and pitch binders could be adjusted for a better production capacity. It was assumed that a limited space inside each barrel of the proposed continuous kneading system was not fully optimized to accommodate green coke-based feed treatment; this exposed the need for further studies on preventing the incineration of feeds with higher volatile matter; notably, green cokes are more affordable in meeting the demands of the current industry, and can achieve higher discharge capacities and ICEs. In a future study, the installation of more discharge outlets between the heating compartments can be considered based on a more detailed analysis of volatile matter dynamics. The 10- μm Pet. showed a commercially acceptable level of a third discharging capacity of 353.1 mAh/g and ICE of 93.7% and its narrow particle size distribution, represented by the highest tap density and lowest surface area, which could be useful in the production of electrodes with more acceptable performances. The 6- μm Pet. (agglomerated structure comprising D50) showed the highest discharging capacity; however, its lower ICE implied a lower compounding effect, which can be attributed to its lower tap density and higher surface area. However, both 10- and 6- μm coals showed below the commercial level of third discharge capacity, probably due to their lower compounding effect of the coal-derived binder, which left many primary particles unaffected and intact.

4. Conclusions

This work proposed an artificial graphite manufacturing process that can minimize the generation of harmful volatile material. Two distinct types of parallel co-rotating twin-screw extruders, namely the KRC-S2 model (Kurimoto. Ltd., Japan) and CHT-20 model (Nanjing Cowin Extrusion Machinery Co., Ltd., China), were selected for this study. Their kneading performances were evaluated at the same residence time at 250 °C. CHT-20 yielded better secondary particle expansion of D50. Subsequently, a retrofit design was conceived by installing an additional component into the CHT-20. It was verified that a smaller diameter combined with a longer screw facilitated the kneading performance. Various premixed feeds of cokes and binding pitch were inserted into the retrofitted kneading system at a temperature higher than that of the softening pitch by 100 °C. The feeds were heat treated and graphitized at 3200 °C. The retrofitted extruder assembly demonstrated effective control of the intrinsic volatiles when kneading the cokes and pitch. In a specific case, the resulting calcined cokes showed a 47% increase in the particle size distribution with no signs of smoke. Additionally, the anode materials presented the highest discharging capacity of more than 350 mAh/g and 90% of ICE.

Author Contributions: Conceptualization, G.-H.L. and S.-M.P.; methodology, G.-H.L. and H.Y.; software, G.-H.L. and H.Y.; validation, G.-H.L.; formal analysis, G.-H.L., J.-M.Y., S.-Y.C. and S.-M.P.; investigation, S.-J.Y., Y.-J.K., D.-J.S. and H.-R.C.; resources, S.-H.Y. and J.-I.P.; data curation, G.-H.L.; writing—original draft preparation, G.-H.L. and K.O.; writing—review and editing, H.Y., Y.-J.K. and H.-R.C.; visualization, G.-H.L. and K.O.; supervision, S.-H.Y. and J.-I.P.; project administration, S.-H.Y. and J.-I.P. All authors have read and agreed to the published version of the manuscript.

Funding: National Research Foundation of Korea (NRF) funded by the Ministry of Education (MOE) (2021RIS-004).

Data Availability Statement: The data presented in this study are available upon request from the corresponding author.

Acknowledgments: These results were supported by the “Regional Innovation Strategy (RIS)” through the National Research Foundation of Korea (NRF) funded by the Ministry of Education (MOE) (2021RIS-004).

Conflicts of Interest: The authors declare no conflict of interest.

References

1. Kim, J.S.; Pflieger, W.; Kohler, R.; Seifert, H.J.; Kim, T.Y.; Byun, D.J.; Jung, H.G.; Choi, W.C.; Lee, J.K. Three-dimensional silicon/carbon core-shell electrode as an anode material for lithium-ion batteries. *J. Power Source* **2015**, *279*, 13–20. [[CrossRef](#)]
2. Scrosati, B.; Garche, J. Lithium batteries: Status, prospects and future. *J. Power Source* **2010**, *195*, 2419–2430. [[CrossRef](#)]
3. Dunn, B.; Kamath, H.; Tarascon, J.M. Electrical energy storage for the grid: A battery of choices. *Science* **2011**, *334*, 928–935. [[CrossRef](#)] [[PubMed](#)]
4. Nishi, Y. Lithium ion secondary batteries; past 10 years and the future. *J. Power Source* **2001**, *100*, 101–106. [[CrossRef](#)]
5. Tarascon, J.M.; Armand, M. Issues and challenges facing rechargeable lithium batteries. *Nature* **2001**, *414*, 359–367. [[CrossRef](#)]
6. Andre, D.; Hain, H.; Lamp, P.; Maglia, F.; Stiaszny, B. Future high-energy density anode materials from an automotive application perspective. *J. Mater. Chem. A* **2017**, *5*, 17174–17198. [[CrossRef](#)]
7. Bresser, D.; Hosoi, K.; Howell, D.; Li, H.; Zeisel, H.; Amine, K.; Passerini, S. Perspectives of automotive battery R&D in China, Germany, Japan, and the USA. *J. Power Source* **2018**, *382*, 176–178.
8. Armand, M.; Tarascon, J.M. Building better batteries. *Nature* **2008**, *451*, 652–657. [[CrossRef](#)]
9. Goodenough, J.B.; Park, K.S. The Li-ion rechargeable battery: A perspective. *JACS* **2013**, *135*, 1167–1176. [[CrossRef](#)]
10. Nitta, N.; Wu, F.; Lee, J.T.; Yushin, G. Li-ion battery materials: Present and future. *Mater. Today* **2015**, *18*, 252–264. [[CrossRef](#)]
11. Mekonnen, Y.; Sundararajan, A.; Sarwat, A.I. A review of cathode and anode materials for lithium-ion batteries. *SoutheastCon* **2016**, *2016*, 1–6.
12. Oh, Y.J.; Shin, M.C.; Kim, J.H.; Yang, S.J. Facile preparation of ZnO quantum dots@porous carbon composites through direct carbonization of metal-organic complex for high-performance lithium ion batteries. *Carbon Lett.* **2021**, *31*, 323–329. [[CrossRef](#)]
13. Zanini, M.; Basu, S.; Fischer, J.E. Alternate Synthesis and Reflectivity Spectrum of Stage 1 Lithium-Graphite Intercalation Compound. *Carbon* **1978**, *16*, 211–212. [[CrossRef](#)]
14. Guerard, D.; Herold, A. Intercalation of lithium into graphite and other carbons. *Carbon* **1975**, *13*, 337–345. [[CrossRef](#)]

15. Basu, S.; Zeller, C.; Flanders, P.J.; Fuerst, C.D.; Johnson, W.D.; Fischer, J.E. Synthesis and properties of lithium-graphite intercalation compounds. *Mater. Sci. Eng.* **1979**, *38*, 275–283. [[CrossRef](#)]
16. Ohta, N.; Nagaoka, K.; Hoshi, K.; Bitoh, S.; Inagaki, M. Carbon-coated graphite for anode of lithium ion rechargeable batteries: Graphite substrates for carbon coating. *J. Power Source* **2009**, *194*, 985–990. [[CrossRef](#)]
17. Han, Y.J.; Kim, J.; Yeo, J.S.; An, J.C.; Hong, I.P.; Nakabayashi, K.; Miyawaki, J.; Jung, J.D.; Yoon, S.H. Coating of graphite anode with coal tar pitch as an effective precursor for enhancing the rate performance in Li-ion batteries: Effects of composition and softening points of coal tar pitch. *Carbon* **2015**, *94*, 432–438. [[CrossRef](#)]
18. Zheng, H.; Kim, M.S. Performance of modified graphite as anode material for lithium-ion secondary battery. *Carbon Lett.* **2011**, *12*, 243–248. [[CrossRef](#)]
19. Shaker, M.; Ghazvini, A.A.S.; Qureshi, F.R.; Riahifar, R. A criterion combined of bulk and surface lithium storage to predict the capacity of porous carbon lithium-ion battery anodes: Lithium-ion battery anode capacity prediction. *Carbon Lett.* **2021**, *31*, 985–990. [[CrossRef](#)]
20. Asenbauer, J.; Eisenmann, T.; Kuenzel, M.; Kazzazi, A.; Chen, Z.; Bresser, D. The success story of graphite as a lithium-ion anode material—Fundamentals, remaining challenges, and recent developments including silicon (oxide) composites. *Sustain. Energy Fuels* **2020**, *4*, 5387–5416. [[CrossRef](#)]
21. Flandrois, S.; Simon, B. Carbon materials for lithium-ion rechargeable batteries. *Carbon* **1999**, *37*, 165–180. [[CrossRef](#)]
22. Lu, M.; Cheng, H.; Yang, Y. A comparison of solid electrolyte interphase (SEI) on the artificial graphite anode of the aged and cycled commercial lithium ion cells. *Electrochim. Acta* **2008**, *53*, 3539–3546. [[CrossRef](#)]
23. Shi, M.; Song, C.; Tai, Z.; Zou, K.; Duan, Y.; Dai, X.; Sun, J.; Chen, Y.; Liu, Y. Coal-derived synthetic graphite with high specific capacity and excellent cyclic stability as anode material for lithium-ion batteries. *Fuel* **2021**, *292*, 120250. [[CrossRef](#)]
24. Singh, B.; Mulvaney, S.J. Modeling and Process Control of Twin-Screw Cooking Food Extruders. *J. Food Eng.* **1994**, *23*, 403–428. [[CrossRef](#)]
25. Kim, S.M.; Woo, J.H.; Kim, H.W.; Park, H.J. Formulation and evaluation of cold-extruded chocolate ganache for three-dimensional food printing. *J. Food Eng.* **2022**, *314*, 110785. [[CrossRef](#)]
26. Snel, S.J.E.; Bellwald, Y.; Goot, A.J.V.D.; Beyrer, M. Novel rotating die coupled to a twin-screw extruder as a new route to produce meat analogues with soy, pea and gluten. *Innov. Food Sci. Emerg. Technol.* **2022**, *81*, 103152. [[CrossRef](#)]
27. Ge, X.; Duan, H.; Zhou, Y.; Zhou, S.; Shen, H.; Liang, W.; Sun, Z.; Yan, W. Mechanistic insights into the supramolecular structure and physicochemical properties of twin-screw extruded high amylose corn starch with different amylose content by improved electron beam irradiation. *Innov. Food Sci. Emerg. Technol.* **2023**, *87*, 103414. [[CrossRef](#)]
28. Riaz, M.N. Chapter 19 Food Extruders. In *Handbook of Farm, Dairy and Food Machinery Engineering*, 3rd ed.; Springer: Berlin/Heidelberg, Germany, 2019; pp. 483–497.
29. Bertan, F.M.; Montedo, O.R.K.; Rambo, C.R.; Hotza, D.; Novaes de Oliveira, A.P. Extruded ZrSiO₄ particulate-reinforced LZSA glass-ceramics matrix composite. *J. Mater. Process. Technol.* **2009**, *209*, 1134–1142. [[CrossRef](#)]
30. Moon, Y.W.; Shin, K.H.; Koh, Y.H.; Choi, W.Y.; Kim, H.E. Porous alumina ceramics with highly aligned pores by heat-treating extruded alumina/camphene body at temperature near its solidification point. *J. Eur. Ceram. Soc.* **2012**, *32*, 1029–1034. [[CrossRef](#)]
31. Tan, D.W.; Guo, W.M.; Lao, Z.Y.; Lin, R.L.; Lin, H.T. A novel strategy for c-axis textured silicon nitride ceramics by hot extrusion. *J. Eur. Ceram. Soc.* **2021**, *41*, 6059–6063. [[CrossRef](#)]
32. Hossain, S.S.; Lu, K. Recent progress of alumina ceramics by direct ink writing: Ink design, printing and post-processing. *Ceram. Int.* **2023**, *49*, 10199–10212. [[CrossRef](#)]
33. Kim, H.; Oh, K.; Seo, Y. Rheological and mechanical properties of a novel polyamide 6 synthesized by anionic polymerization of ε-caprolactam in a twin-screw extruder. *Polymer* **2019**, *177*, 196–201. [[CrossRef](#)]
34. McGauran, T.; Harris, M.; Dunne, N.; Smyth, B.M.; Cunningham, E. Development and optimisation of extruded bio-based polymers from poultry feathers. *Eur. Polym. J.* **2021**, *158*, 110678. [[CrossRef](#)]
35. Chen, Y.C.; Moseson, D.E.; Richard, C.A.; Swinney, M.R.; Horava, S.D.; Oucherif, K.A.; Cox, A.L.; Hawkins, E.D.; Li, Y.; DeNeve, D.F.; et al. Development of hot-melt extruded drug/polymer matrices for sustained delivery of meloxicam. *J. Control. Release* **2022**, *342*, 189–200. [[CrossRef](#)] [[PubMed](#)]
36. Roland, W.; Hammer, A.; Leimhofer, C.; Kapshammer, A.; Hild, S. Application of a novel testing device to characterize the layer adhesion of co-extruded polymer sheets. *Mater. Today Proc.* **2022**, *62*, 2652–2657. [[CrossRef](#)]
37. Fujita, Y.; Fukumoto, K.; Agata, H.; Fukui, T. Development of Continuous Kneading Process for Cathode Electrode of Lithium-Ion Battery. *J. Soc. Powder Technol. Jpn.* **2014**, *51*, 206–211. [[CrossRef](#)]

Disclaimer/Publisher’s Note: The statements, opinions and data contained in all publications are solely those of the individual author(s) and contributor(s) and not of MDPI and/or the editor(s). MDPI and/or the editor(s) disclaim responsibility for any injury to people or property resulting from any ideas, methods, instructions or products referred to in the content.